(Received 23 June 2024, Accepted 4 August 2024, Scheduled 22 August 2024)

A Microwave Subsystem (MS) Capable of Realizing Functional Change With the Aid of 2D-Shaped Liquid Metal (LM)

Xiaochuan Fang[1,*], Shaker Alkaraki[2], and James R. Kelly[3]

[1]James Watt School of Engineering, University of Glasgow, Glasgow, G12 8QQ, UK
[2]George Green Institute for Electromagnetics Research, Department of Electrical and Electronic Engineering University of Nottingham, Nottingham, NG7 2RD, UK
[3]Antennas and Electromagnetics Research Group, School of Electronic Engineering and Computer Science Queen Mary University of London, London E1 4NS, UK

ABSTRACT: This paper presents the first microwave subsystem (MS) capable of changing its function, in this case between resonator and antenna, using liquid metal (LM). This is achieved by filling/emptying fluidic channels with Gallium-based LM and forming LM into different 2D shapes. The manufactured prototype of the proposed MS performs as a slot antenna, when the fluidic channels are empty of LM. On the other hand, it operates in resonator mode, when the fluidic channels are filled with LM. We also connected two MSs along with a microstrip resonator to realize functional change between complex functions, i.e., antenna and filter. The proposed connection of MSs can act as a filter when the fluidic channels are filled with LM or as an antenna when LM is withdrawn from the fluidic channels. When operating in the antenna mode the proposed connection of MSs provides a measured peak realized gain of 7.23 dBi and a simulated total efficiency of 84%. When operating in the filter mode the connection of MSs provides a band-pass response and exhibits a minimum insertion loss of 1.9 dB, within the passband. The filters 10 dB return loss bandwidth, of 340 MHz, ranges from 2.28 GHz to 2.62 GHz.

1. INTRODUCTION

Space within wireless hardware system is at a premium due to the increasing number of radio access technologies that must be supported as well as the trend towards larger display sizes. To address the issue discussed above, there is a need for innovative space saving strategies. On the other hand, some microwave circuits and subsystems, e.g., antennas and filters, are hard to miniaturize whilst maintain a good performance. This is because their performance is obtained from their specific physical geometrical features. A different method to reduce the overall space occupation of these circuits/subsystems in a wireless system is to implement multifunctional/functional changeable circuits/subsystems. Various multifunctional microwave circuits/subsystems, e.g., filtennas, have been reported [1–10]. However, most multifunctional circuits/subsystems are in fact subsystems consisting of components that operate in different functions. For instance, a filtenna consists of a filter into the feedline of an antenna. This is to say, functions in a multifunctional circuits/systems are not able to be operated independently. Consequently, application scenarios of multifunctional circuits/subsystems are limited. So far, there are some reported designs capable of functional change [11–22]. These function changeable circuits/subsystems allow different functions to be operated separately. Nevertheless, all of these designs use the same structure, e.g., a resonant microstrip patch or cascaded circuits, to realize different functions. Those designs therefore need to balance competing performance requirements, for instance, the need to reduce insertion loss within the filter mode whilst enhancing radiation efficiency in the antenna mode. For this reason, the performance of those subsystems will either be outstanding in one function and poor in another, or generally quite poor in both functions.

Interest in using Gallium-based liquid metal (LM), within microwave circuits and antennas, started to grow around 2014 [23, 24]. This was driven by advances in materials science and significant performance advantages associated with the use of LMs. LMs based on alloys of Gallium are non-toxic. LM also has a purely real input impedance, which allows it to be simply implemented in designing circuits/subsystems as well as with a comparable performance against conventional circuits/subsystems. The liquid metal used in the proposed work is EGaIN. It consists of 75.5% Gallium and 24.5% Indium. This material allows the proposed device to have greater power handing capability and lower insertion losses together with enhanced tuning range. Moreover, EGaIN is not toxic and commercially available. It has outstanding electromagnetic features, for example, purely real input impedance and high linearity. It has an electrical conductivity of 3.4×10^6 S/m, which is only one seventeenth of copper.

To date, LM has been mainly used to alter the length of a wire or act as a switch [25–32]. On this basis, real-time tuning based on LM is presented [33, 34]. There are no designs, in the literature, that realize functional change with the aid of LM. However, LM is a very good candidate for building subsystems capable of functional change because it can be formed into 2D shapes. LM is a non-Newtonian fluid [35] and is easily oxidized. This means that LM can be morphed into a variety

* Corresponding author: Xiaochuan Fang (xiaochuan.fang@glasgow.ac.uk).

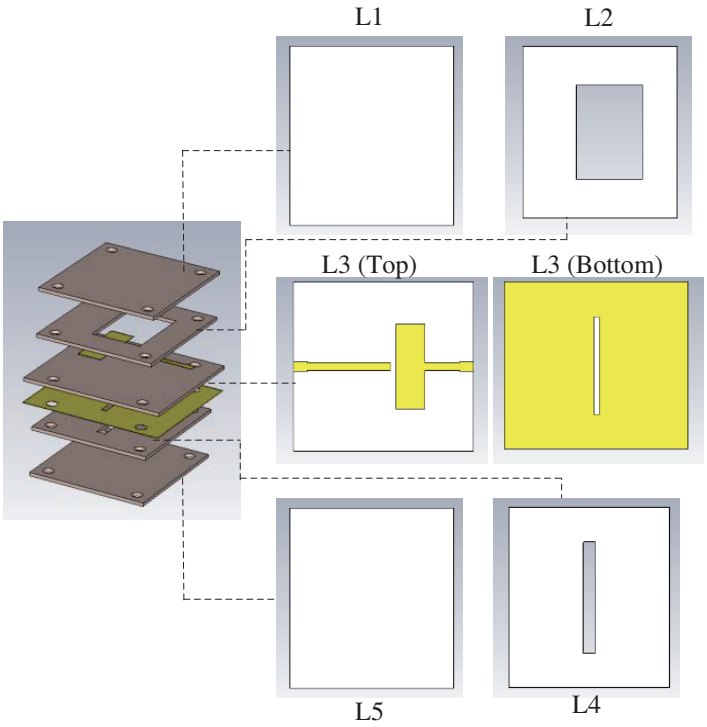

FIGURE 1. Perspective view and layers of the MS. Color Key: substrate = brown, copper = yellow.

of 2D shapes. We could therefore use LM to form 2D geometrical features when required, and totally remove these features by evacuating the LM, when they are no longer needed. In this way, LM allows us to build a subsystem capable of functional change where every function is independent of the others.

Commonly, when 2D-shaped LM is used in microwave device, they are fixed into those devices and is highly unlikely be changed or removed. Very few papers have reported designs that involve moveable 2D-shaped LM. When people wish to do this, they tend to form LM into meandered fluidic channels [36–42]. Meandered channels are much more complex to fabricate, and they have reduced mechanical strength. It should also be noted that this approach cannot be really used to form LM into genuinely 2D shapes unless the walls of the meandered channels are formed from a series of posts with gaps between them. When this is the case, external pressure is applied to the LM, after the channel has been completely filled, in order to force the LM through the gaps between the posts [39–42]. This kind of channel structure tends to be extremely fragile, and it is common for the tiny posts to de-bond from the top and bottom layers of the channel [43].

Since there is a rapid upgrading in wireless communications as well as a boosted number of users' devices, metal waste becomes a severe issue. A microwave device that is able to cope with a change in its function and can be recycled is regarded as a solution. Moreover, resonating/filtering and radiating are two essential functionalities that are required from a hardware in users' devices. To cope with above scenarios, the proposed device displays a microwave device that can change its functionality between resonator and radiator via an approach that possesses reduced metal waste.

This paper presents the first microwave subsystem capable of changing its function using LM. The subsystem can alter its function between resonator (i.e., single-pole filter) and antenna mode. Namely, the proposed subsystem is operated as a conventional slot antenna, when the fluidic channels are empty of LM. It works as a resonator when the fluidic channels are filled with Gallium-based LM. It can also return to antenna mode operation when LM is emptied from fluidic channel. Such function change is repeatable. This paper also shows a more complex functional change by connecting two MSs together via a microstrip patch resonator. The proposed connection of MSs is capable of changing its function between that of a third-order filter and a beam switchable antenna. Akin to the single MS, this is achieved by filling/emptying fluidic channels with LM. Importantly, separate parts of the structure are used to handle different functions. For this reason, the proposed MS and connection of MSs provides good performance in both operating modes (i.e., low insertion loss in the filter mode and high efficiency in the antenna mode).

The paper is organized as follows. Section 2 introduces the concept and configuration of the proposed MS as well as the proposed connection of MSs. Section 3 presents the working principle of the MS and the connection of MSs. Section 4 presents simulation and measurement results for the MS and the connection of MSs when they are operating in different modes.

2. CONCEPT AND STRUCTURE OF A FUNCTION CHANGEABLE MS AND A CONNECTION OF MSS

In this paper, we propose two different subsystems that rely on LM. The first subsystem is a functional changeable microwave

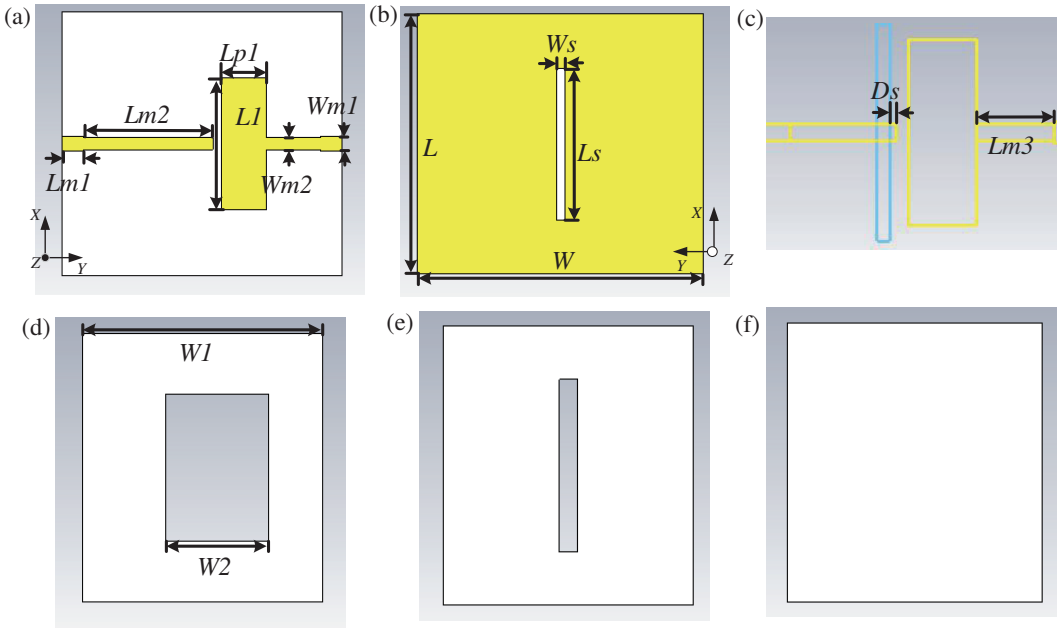

FIGURE 2. Different layers of MS (a) layer 1 with uppermost layer of metallization, (b) layer 1 with lowermost layer of metallization, (c) wireframe view of layer 1, (d) layer 2, (e) layer 3, (f) layer 4&5. Color Key: substrate= white, copper = yellow, radiating slot=blue.

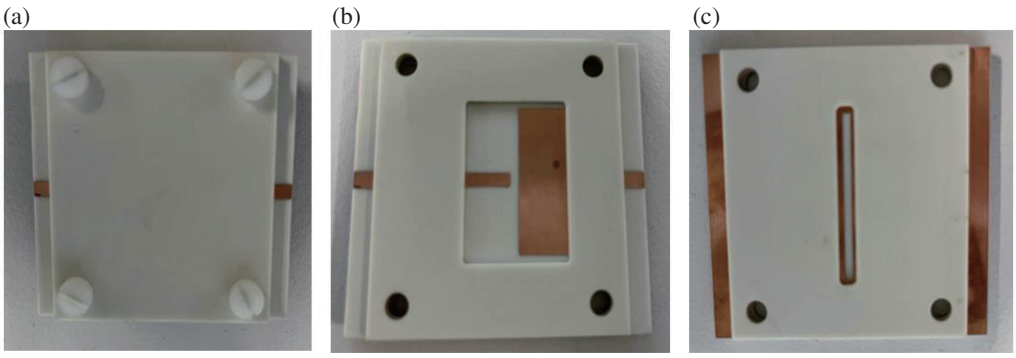

FIGURE 3. The prototype of the proposed MS. (a) Complete assembled MS. (b) Top view without top cover to show the fluidic channel. (c) Bottom view without bottom cover.

subsystem (MS), shown in Figs. 1–3. The proposed functional changeable MS is able to change its function between an antenna and a resonator. Functional change is achieved with the aid of LM. LM is morphed into the shape of the resonator. When LM is emptied from the MS, it operates as a slot antenna. The proposed MS operates at 2.5 GHz.

The second subsystem is a connection of MSs, which is shown in Figs. 4 to 6. The second subsystem is able to change its function between that of a beam switchable antenna and a microwave filter by forming LM in 2D shapes. In the second subsystem, the antenna operates at 2.55 GHz, and the filter has a 10 dB return loss bandwidth of 340 MHz, ranging from 2.28 GHz to 2.62 GHz.

2.1. The MS That Realizes Functional Change Between Antenna and Resonator

The proposed MS realizes functional change between antenna and resonator with the aid of LM. The building block element (BBE) is composed of five substrate layers. Figure 1 shows a perspective view of the proposed MS. In the proposed BBE, substrate layers $L2$, $L3$, and $L4$ are bonded together. This was achieved using a printed circuit board (PCB) bonding film. Substrate layers 4 and 5 are attached using screws, located in the corners of the device. The dimensions of the substrate layers $L1$, $L2$, $L4$, and $L5$ are slightly smaller than those of substrate layer $L3$ (i.e., 5 mm). This is necessary in order to leave sufficient space to mount the SMA connectors. All of the substrate layers are made from a Rogers substrate material, namely RO4003C. RO4003C has a permittivity of 3.55 and a loss tangent of 0.0022 at 10 GHz. The thickness of each substrate layer, i.e., substrate layer $L1$ to substrate layer $L5$, is the same, namely 1.53 mm. The choice of substrate material was influenced by an attempt to balance the requirements of the resonator with those of the antenna. Fig. 2 shows the hardware prototype of the MS.

Figure 3 displays the structure of each layer of the MS. Figs. 3(a) and (b) show layer 1 of the MS. Substrate layer 1

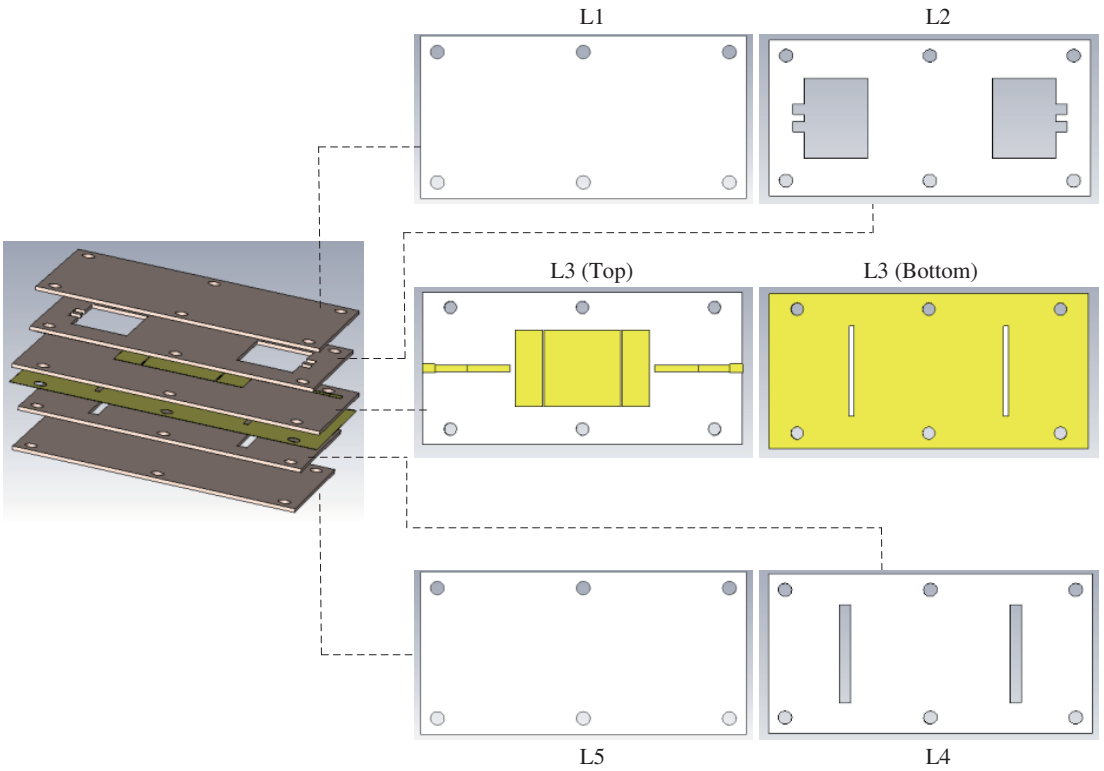

FIGURE 4. (a) Perspective view and layers of the connection of MSs. Color Key: substrate = brown, copper = yellow.

is the only layer of the MS that includes Copper metallization. The resonator and radiator are fabricated on different sides of $L3$. We term the side that incorporates the resonator as the uppermost layer of metallization, and we term the side that incorporates the radiator as the lowermost layer of metallization. Fig. 3(c) shows a wireframe view of substrate $L3$. This wireframe view illustrates the alignment between the uppermost and lowermost layers of metallization. The radiating slot, located on the lowermost layer of metallization, is fed by a microstrip line, which is also printed on the uppermost layer of metallization. The distance between the left end of the microstrip line and the right edge of the slot (denoted Ds) was altered to improve the impedance matching, between the feed line and the slot antenna. Figs. 3(d), (e), and (f) show the structure of $L1$, $L2$, and $L4$ for the MS. $L2$ and $L4$ are located immediately below and above substrate layer 1. Two rectangular channels are etched into the centers of $L2$ and $L4$, respectively. When filled with LM, the first of those channels forms the LM part of the resonator. When filled with LM, the second channel blocks the radiating slot. The fluidic channels are dimensioned so that they slightly overlap the printed metallization on layer 1. This helps to ensure that the LM makes full contact with the printed metallization. Substrate layers 4 and 5 are located at the top and bottom of the MS, respectively. Those two layers are identical to one another, as shown in Fig. 3(f). $L1$ and $L5$ serve as covers for the fluidic channels, which prevent the LM from leaking out.

The microstrip line consists of two sections, each of which has a different width. There is no substrate material above the wide sections of the microstrip line, and consequently they are conventional single layer microstrip structures. For this reason, their widths can be calculated using the well-known equation. The thin microstrip lines, on the other hand, are covered by a superstrate layer (namely: substrate layer 2). For this reason, a different approach is needed to calculate the width (denoted w) of these microstrip lines. In particular, we employ (1) [44].

$$Z_0 = \frac{60}{\sqrt{\varepsilon_e}} \ln\left(\frac{8H}{w} + \frac{w}{4d}\right) \tag{1}$$

In this design, $\varepsilon_e = \varepsilon_r$ [45] where ε_r is the permittivity of RO4003C, namely 3.55.

Table 1 gives the dimensions of the proposed MS. The dimensions are very close to the values calculated using the well-known theory [44]. All of the layers of the proposed MS are easy to manufacture using standard PCB fabrication methods.

2.2. A Connection of MSs That Realizes Functional Change between Antenna and Filter

In this subsection, we discuss a connection of MSs which can realize more complex functional change, i.e., between filter and antenna functions, with the aid of LM. Fig. 4 shows the configuration of the proposed connection of MSs. Just like single MS, this connection of MSs is composed of five substrate layers. The structure of each layer is identical to that of the single MS that was introduced in the previous section. When the relevant channels are filled with LM, they can be used to realize the first/last resonators within the filter. The resonator, located in the center of the uppermost layer of metallization, was implemented using a Copper patch. This Copper patch was intro-

FIGURE 5. The prototype of connection of MSs. (a) Complete assembled interconnection of MSs. (b) Top view without top cover to show the fluidic channel. (c) Bottom view without bottom cover.

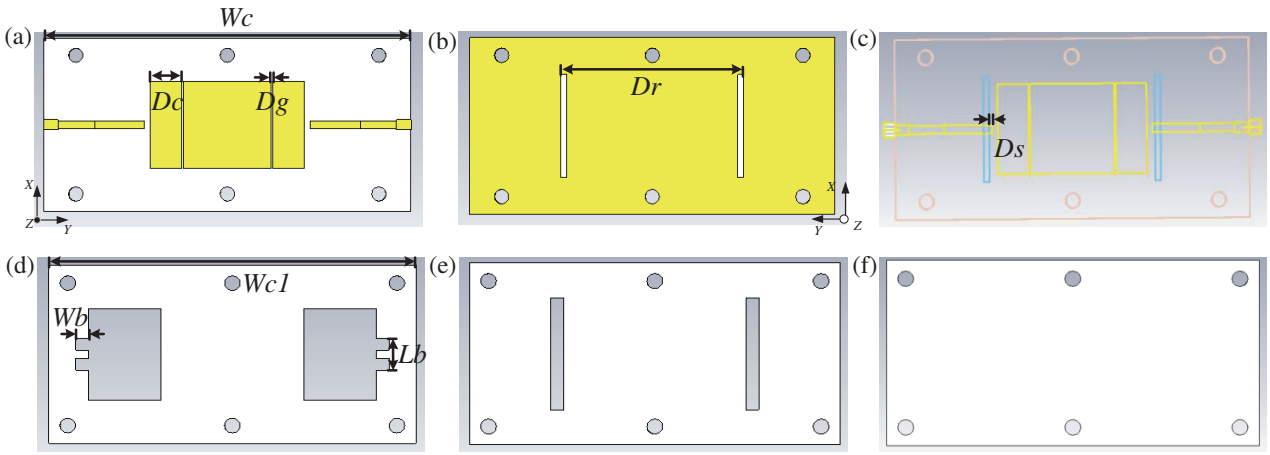

FIGURE 6. Different layers of the connection of MSs, (a) substrate layer 1 with uppermost layer of metallization, (b) substrate layer 1 with lowermost layer of metallization, (c) wireframe view of substrate layer 1, (d) substrate layer 2, (e) substrate layer 3, (f) substrate layer 4 & 5. Color Key: substrate = white, copper = yellow, radiating slot = blue.

TABLE 1. Dimensions of the MS (mm).

$W = 65$	$L = 60$	$W1 = 19$	$L1 = 30$	$W2 = 20$
$Lp1 = 11$	$Ws = 2$	$Ls = 35$	$Lm1 = 5$	$Lm2 = 29.5$
$Lm3 = 12.5$	$Wm1 = 3.37$	$Wm2 = 2.76$	$Ds = 1$	

duced to produce a 3-pole filter. Theoretically, this central resonator could also be created by LM. However, if we did that the distance between the first/last resonators would be insufficient, and there would be a high risk of the LM, in adjacent fluidic channels, merging together. Two radiating slots are located on the lowermost layer. Those radiating slots are designed to radiate independently, with opposite phase to one another. When the fluidic channels are emptied of LM, these slots enable the connection of MSs to perform as a beam switchable antenna. Fig. 5 shows the hardware prototype of the connection of MSs.

Figure 6 shows the structure of each layer within the connection of MSs. Figs. 6(a) and (b) show $L3$ within the connection of MSs. Akin to the single MS, $L3$ is the only layer within the connection of MSs that includes Copper metallization. Fig. 6(c) shows a wireframe view of $L3$. Fig.6(d) illustrates layer 2. It can be seen that three square microfluidic channels are etched into layer 2. When those channels are filled, they form two resonators. These resonators are the resonators within the filter. $L2$ is bonded to the uppermost layer of metallization, associated with layer 1 as shown in Fig. 6(e), and $L4$ is bonded to the lowermost layer of metallization. The two rectangular channels, etched into this layer, are located below the radiating slots. In turn, the radiating slots are etched into the ground plane. In other words, the LM within the rectangular channels is used to cover these radiating slots and create a solid metal ground plane. Akin with the single MS, two cover layers, shown in Fig. 6(f), are used to prevent LM from leaking out of the fluidic channels. These cover layers are substrates $L1$ and $L5$. Once again, they were attached to the other layers using screws, making them easy to fit and remove. Table 2 gives the dimensions of the proposed connection of MSs.

TABLE 2. Dimensions of the connection of MSs (mm).

$Wc = 126$	$Lc = 60$	$Dg = 0.5$
$Ds = 0.5$	$Dc = 8$	$Wb = 4$
$Dr = 61$	$Lb = 10.76$	$Wc1 = 116$

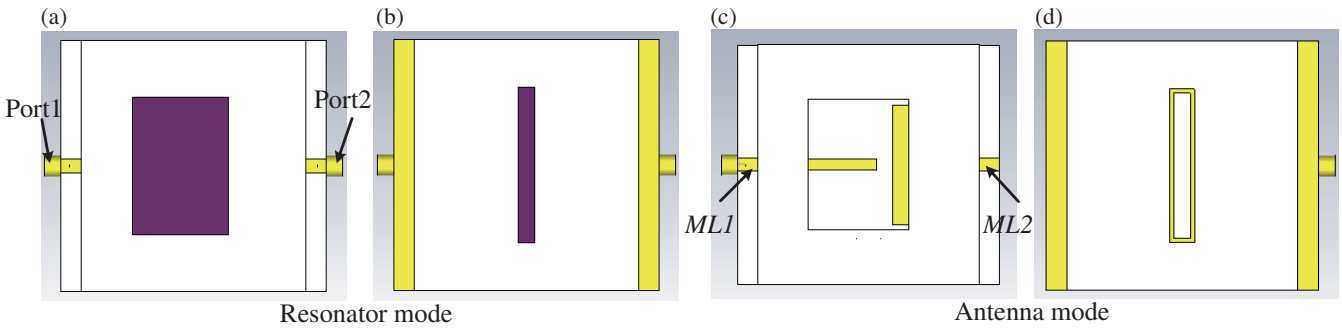

FIGURE 7. (a) Top and (b) bottom view of the MS (resonator mode). (c) Top and (d) bottom view of the MS (antenna mode). Color Key: substrate= white, copper = yellow, LM = purple.

3. WORKING PRINCIPLE OF A FUNCTIONAL CHANGEABLE MS/CONNECTION OF MSS

In this section, we present the working principle of a microwave subsystem (MS) connection of MS capable of functional change. The proposed MS realizes functional change between resonator mode and antenna mode. The proposed connection of MSs realizes functional change between filter mode and antenna mode. In both cases, functional change is realized with the aid of 2D-shaped LM. Namely the MS/connection of MSs are operating in antenna mode when they are empty of LM. The MS/connection of MSs operate in resonator/filter mode when the fluidic channels within them are filled with LM. We chose to use a Gallium-based LM called EGaIN for this research. EGaIN has an electrical conductivity of 3.4×10^6 S/m [46].

3.1. A MS That Realizes Functional Change Between Resonator and Antenna

The proposed MS can be switched between resonator mode and antenna mode. The resonator mode of the proposed MS is realized by filling fluidic channels with LM. Specifically, we fill the fluidic channels in substrate layer 2 and substrate layer 3, as shown in Figs. 7(a) and (b). Once these channels have been filled, the proposed MS operates as a microstrip patch resonator. On the other hand, the antenna mode of the MS is realized by emptying all of the fluidic channels of LM, as shown in Figs. 7(c) and (d). Under this circumstance, the proposed MS operates as a planar slot antenna.

Figures 7(a) and (b) show the top and bottom views of the MS when it is operating in the resonator mode. For this scenario, the uppermost layer of metallization consists of a resonator and two Copper microstrip lines (denoted *ML1* and *ML2*). The MS is excited by two ports positioned at the far ends of the two microstrip lines. The resonator consists of a block of LM (shaded in purple) and a Copper patch (shaded in yellow). The LM block is created by filling the rectangular fluidic channel, located in the center of substrate layer 2, with LM. Part of the Copper patch is located beneath the LM thus ensuring adequate electrical contact with the LM. The reason for employing this Copper patch is to obtain reliable and reproducible results when a number of MSs are cascaded to form a connection of MSs, and this will be explained in greater detail in the next section. Similarly, the lowermost layer of metallization becomes a solid ground plane when the relevant fluidic channels are filled with LM. The fluidic channels that need to be filled to create a solid ground plane are etched into substrate layer 3. Under this scenario, the uppermost layer of metallization is configured to operate as a microstrip resonator.

Figures 7(c) and (d) show the top and bottom views of the MS when it is configured to operate in the antenna mode. This is achieved when LM is emptied from all fluidic channels. The uppermost layer of metallization consists of two microstrip lines and a Copper patch. Microstrip lines *ML1* and *ML2* are tap coupled to the resonator. The lowermost layer of metallization forms the ground plane of the MS. This layer incorporates a slot. Please note that *ML1* (which is located on the uppermost layer of metallization) overlaps the slot on the lowermost layer of metallization. These are the only two features, on those layers, which overlap. This design ensures that the uppermost layer of metallization will not affect the radiation from the slot located on the lowermost layer of metallization. When the MS operates in the antenna mode, LM is emptied from all of the fluidic channels. The lowermost layer of metallization is thus configured to operate as a slot antenna. The slot radiator, in the proposed MS, is fed by *ML1* which is located on the uppermost layer of metallization.

When the proposed MS operates in the resonator mode, it makes use of a microstrip patch resonator. The design methodology for this resonator is given in most textbooks on microwave engineering [44]. The same textbook theory tells us that the operating frequency of the proposed MS is inversely proportional to the length of the resonator (i.e., *L1*). The width of the resonator (*W1*) influences the transmission coefficient, i.e., S_{21}. The proposed MS is designed to operate at 2.5 GHz. The choice of operating frequency is not influenced by any specific requirement, but rather it was chosen for proof-of-concept demonstration. If a different operating frequency were required, then the dimensions of the LM patch resonator, as well as the radiating slot, could be easily redesigned, using established and well-known theory [39].

When the proposed MS operates in the antenna mode, it behaves as a slot antenna. The design methodology of the slot antenna is given in standard textbooks on microwave engineering [48]. The operating frequency of the proposed MS is de-

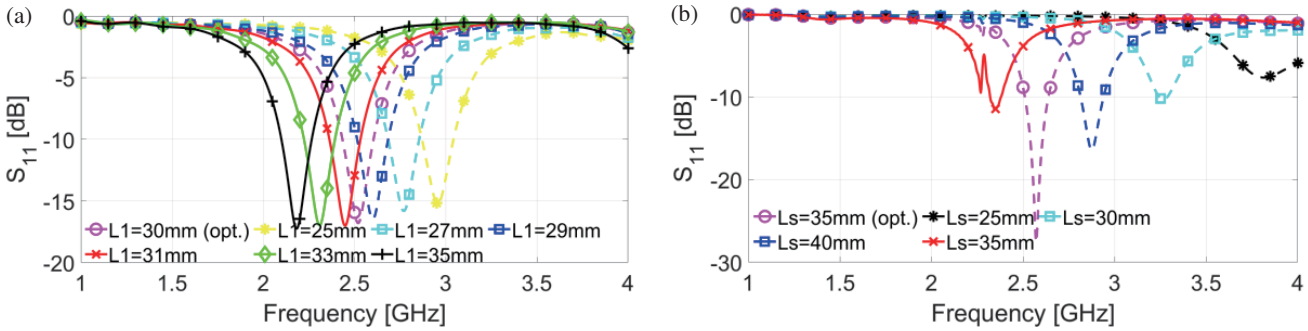

FIGURE 8. (a) Parametric study of S_{11} of the MS (resonator mode) when change the $L1$. (b) Parametric study of S_{11} of the MS (antenna mode) when change the Ls.

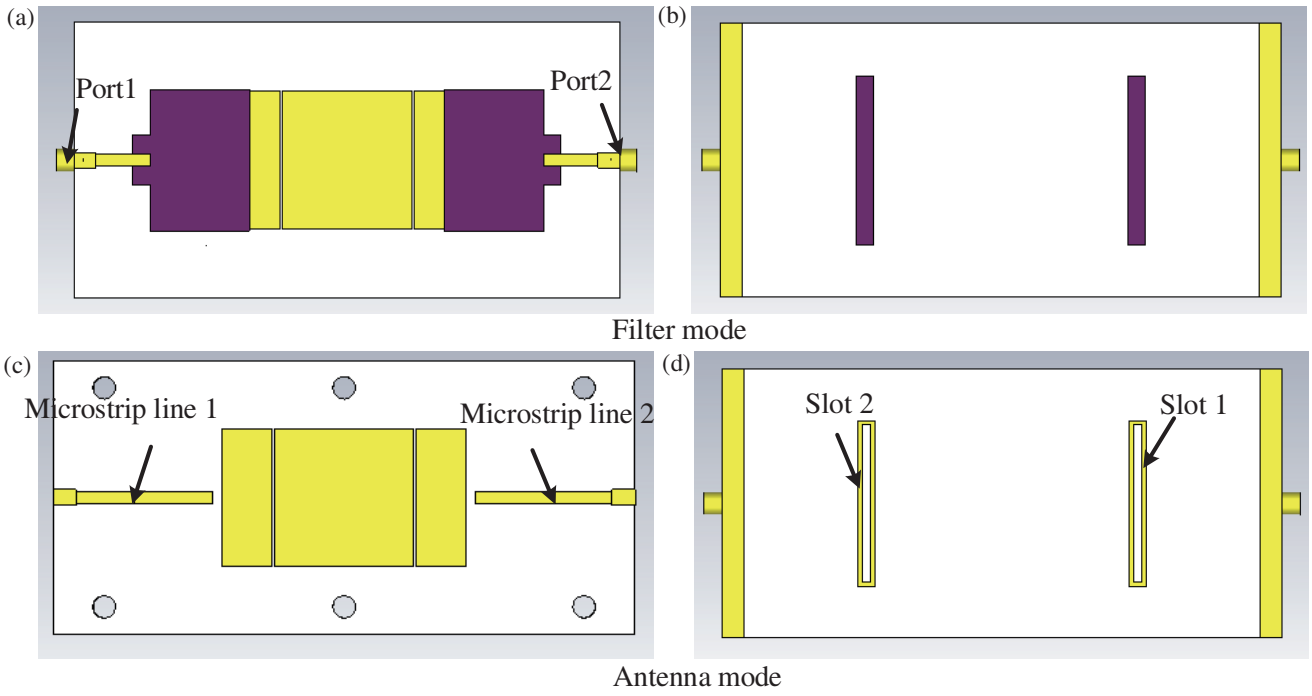

FIGURE 9. (a) Top and (b) bottom view of the connection of MSs (filter mode). (c) Top and (d) bottom view of the connection of MSs (antenna mode). Color Key: substrate = white, copper = yellow, LM = purple.

termined by the length of the radiating slot (*Ls*), as shown in Fig. 8(b) [48]. The width of the radiating slot (i.e., *Ws*) influences the bandwidth as well as the impedance matching of the MS, in the antenna mode. A wider radiating slot improves those two factors [44].

A slot antenna produces bi-directional radiation. However, in many practical applications, antennas are required to have uni-directional beams and be attached to a metal surface. For these reasons, when the MS/connection of MSs is operated in the antenna mode, a reflector is placed below the lowermost layer of metallization. The distance between the reflector and layer 1 was chosen to be closed to a quarter of a free-space wavelength at the center frequency of 2.5 GHz. A rectangular block of Rohacell foam was employed to support this reflector by sticking layer 4 of the MS/connection of MSs and reflector together. It should be emphasized here that we could remove the reflectors from the proposed MS/connection of MSs. The main effect of this would be to cause the radiation pattern, in the antenna mode, to be omnidirectional. The total efficiency of the MS/connection of MSs would not be affected. However, the peak gain would reduce significantly, due to the change in the shape of the radiation pattern.

3.2. A Connection of MSs That Realizes Functional Change between Filter and Antenna

This subsection presents a scenario where functional change is realized within a connection of cascaded MSs. Specifically, we show that by cascading two MSs and a microstrip patch resonator, we can realize functional change between a third order bandpass filter and a beam switchable antenna.

Figures 9(a) and (b) show the top and bottom views of the connection of MSs when it is configured to operate in filter

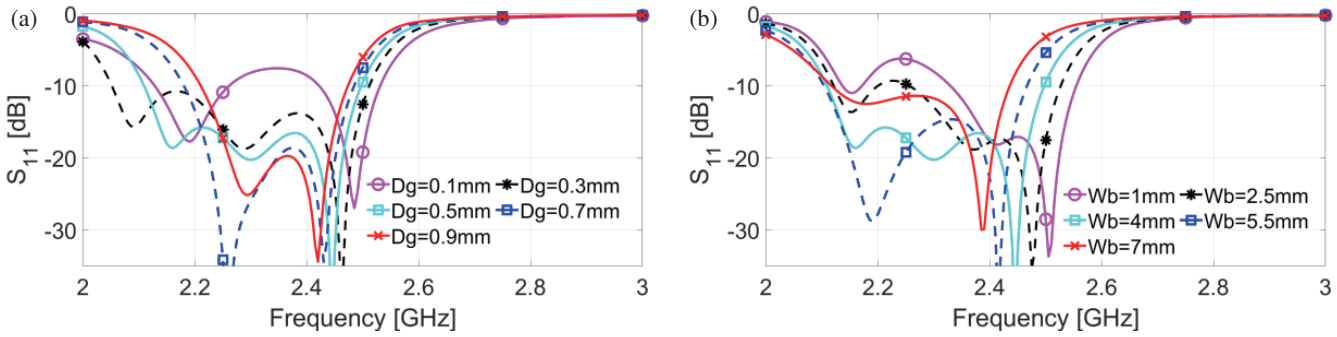

FIGURE 10. (a) Parametric study on S_{11} of the connection of MSs (filter mode) when changing Dg. (b) Parametric study of S_{11} of the connection of MSs (filter mode) when changing Wb.

mode. When all of the fluidic channels are filled with LM, the proposed connection of MSs operates as a third order filter, based around rectangular microstrip patch resonators. This kind of filter can be designed and analyzed using the well-known insertion loss method, covered in most textbooks on microwave engineering [36]. The coupling coefficient of the filter is mainly controlled by the size of the gaps between the patches (denoted *Dg*). In the proposed connection of MSs, *Dg* is firstly calculated by a method given in [48], and it is subsequently optimized in Computer Simulation Technology (CST). We also performed a parametric study for *Dg*, and the result is given in Fig. 10(a). When *Dg* increases, the coupling coefficient between the resonators increases. Subsequently, the fractional bandwidth (FBW) of this connection of MSs (filter mode) is increased. Recall that in the MS, part of the resonator is made up of a Copper patch. In this connection of MSs, this Copper patch enables a sufficient distance between LM resonator and microstrip patch in the center of upper most layer of metallization, which provides a safe area for possible LM leaks. The separation distance between the fluidic channels and the neighboring gap (denoted *Dc*) is 8 mm. This separation distance ensures that, even if LM leaks from the fluidic channel, it will not block the gaps between resonators. This enables the necessary mutual coupling to be set up between the resonators.

In order to produce the required input and output quality factors, for the filter, two bars of LM were added above the junctions between the first/last patch elements and the associated microstrip lines (see Fig. 9(a)). The length and width of the LM bar (denoted *Wb* and *Lb*) were adjusted until three zeros could be observed in the S_{11} curve. The required values of *Wb* and *Lb* were determined through a parametric study, performed in CST Microwave Studio. Fig. 10(b) presents the results obtained through the parametric study on *Wb*. It can be observed that as *Wb* is increased the FBW of connection of MSs, operating in the filter mode, is reduced. On the other hand, when *Wb* increases, the value of S_{11}, within the filter's passband, improves (i.e., becomes a larger negative number), and the three S_{11} zeros become more equal in their magnitudes. The parametric study on *Lb* reveals a similar trend. Akin to the case of the MS, the connection of MSs operates in filter mode when the fluidic channels, used to cover the radiating slots, are filled with LM. Under this condition, the lowermost layer of metallization, associated with substrate layer 1, acts as a solid ground plane.

When all of the fluidic channels are emptied of LM, the proposed connection of MSs operates as a beam switchable antenna. Each of the radiating slots is excited independently and produces a beam, tilted towards a different direction. The working principle of the slot antenna is akin to that for the single MS. Figs. 9(c) and (d) show the top and bottom views of the connection of MSs, when it operates in the antenna mode. It can be seen that, akin to the case of the MS, the radiating slots are fed via microstrip lines. Specifically, slot 1 and slot 2 are fed by the two microstrip lines, i.e., microstrip line 1 and microstrip line 2. Those two slots are excited separately with opposite phases. Each of the slots produces a main beam directed at an angle of 30° from boresight. The value of *Ds* is the same for slot 1 and slot 2.

4. SIMULATION AND MEASUREMENT RESULTS

This section presents simulation and measurement results for the proposed microwave subsystem (MS) as well as for the connection of MSs. First, we present results for the antenna mode. This mode is obtained when all of the fluidic channels are emptied of LM, as discussed above. The S-parameters of the antenna mode MS and connection of MSs were measured using a vector network analyzer (namely a PNA-L from Keysight Technologies). The radiation patterns were measured in an anechoic chamber. The realized gain of the MS/connection of MSs was measured using the gain comparison method. After measuring the performance of the MS/connection of MSs in the antenna mode, Gallium-based LM was injected into the fluidic channels in order to configure the structures for operation in resonator/filter mode. The S-parameters of the resonator/filter mode for the single MS and the interconnection of the MSs were then measured.

4.1. Antenna Mode MS/Connection of MSs

In this subsection, we present the performance of the MS and the connection of MSs when they are configured to operate in antenna mode. In the antenna mode, the proposed MS and connection of MSs does not incorporate LM. Fig. 11 shows a prototype of the antenna mode MS/connection of MSs with the

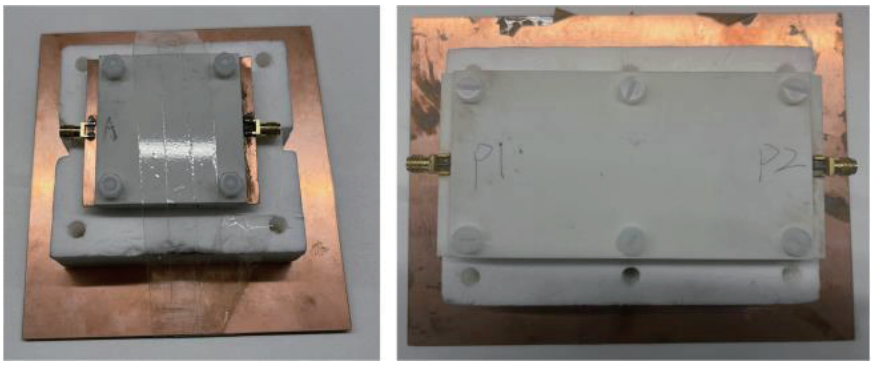

FIGURE 11. MS/connection of MSs with Rohacell and reflector (antenna mode).

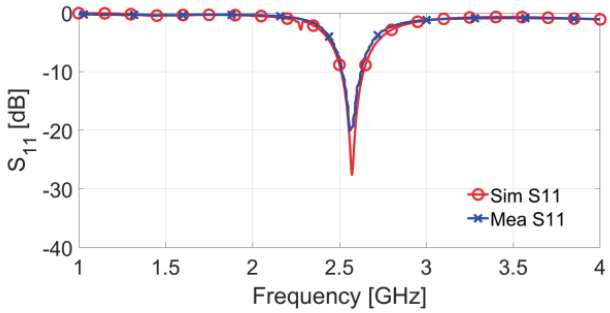

FIGURE 12. S_{11} for the single MS operating in antenna mode. Where: Sim. Means simulated and Meas. means measured.

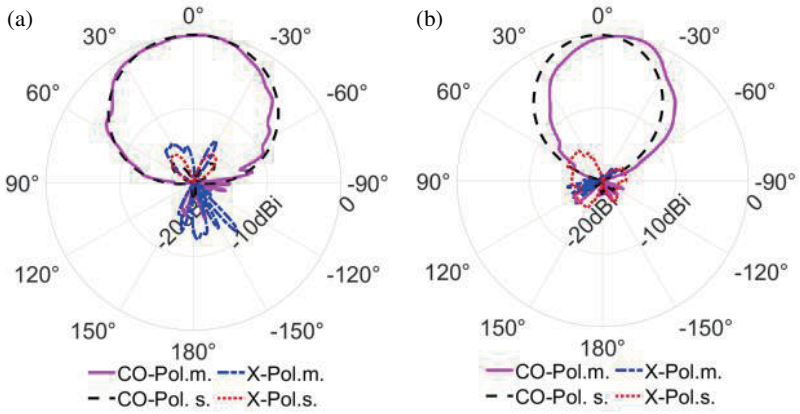

FIGURE 13. Normalized radiation patterns for the single MS when it is operating in antenna mode: (a) E-plane, (b) H-plane. Where: CO-Pol. means co-polarization, X-Pol. means cross polarization, Sim. means simulated and Meas. means measured.

reflector attached, as explained in previous section. When the proposed single MS is operating in the antenna mode, the radiating slot of the MS is fed by *ML1*. In this case, the MS will be excited by port 1. A 50 Ω matched load will be connected to port 2.

Figure 12 presents the simulated and measured S_{11} of the MS, operating in antenna mode. The simulated resonant frequency is 2.56 GHz. The measured resonant frequency is 2.57 GHz. The difference between simulation and measurement is therefore 0.39%, which is acceptable.

Figure 13 presents the normalized E-plane and H-plane radiation patterns for the MS when it is operating in antenna mode. Please note that the xz-plane (see Fig. 2) is equivalent to the E-plane, whilst the yz-plane is equivalent to the H-plane. The measured radiation patterns are in good agreement with the simulated ones. The simulated total efficiency of the antenna mode is 95.4%. The simulated peak realized gain of the antenna mode MS is 8.74 dBi, and the measured peak realized gain of antenna mode MS is 7.81 dBi. The difference between simulated and measured peak realized gains is 0.93 dBi. The gain difference

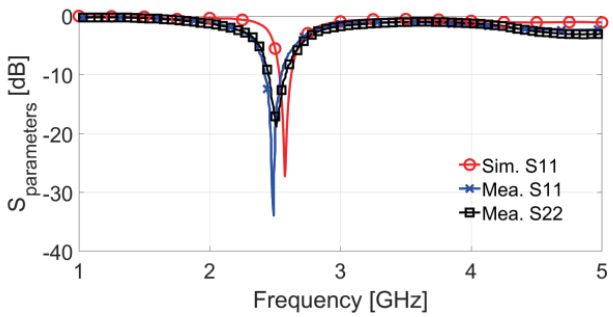

FIGURE 14. S-parameters for the connection of MSs operating in antenna mode. Where: Sim. Means simulated and Meas. means measured.

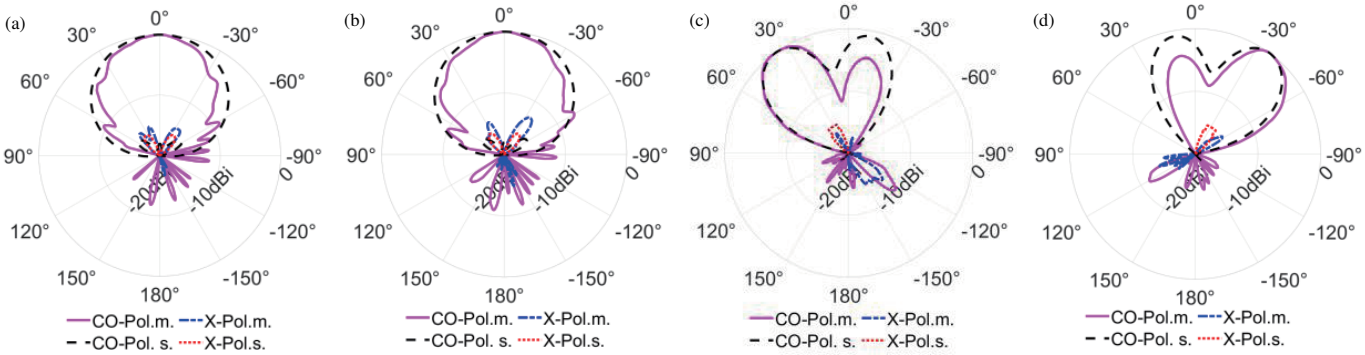

FIGURE 15. Normalized radiation patterns for the connection of MSs when it is operating in antenna mode: (a) E-plane for slot1, (b) E-plane for slot2 (c) H-plane for slot 1, (d) H-plane for slot 2. Where: CO-Pol. means co-polarization, X-Pol. means cross polarization, Sim. means simulated and Meas. means measured.

is mostly caused by assembly errors, as the proposed MS is a five-layer structure with Rohacell foam supporter and reflector.

Figure 14 presents the simulated and measured S-parameters of the antenna mode connection of MSs. Sim. S_{11} indicates the simulated reflection coefficients of slots 1 and 2. Please note that the simulated reflection coefficients of the two slots should overlap with one other. Mea. S_{11} denotes the measured reflection coefficient of slot 1. Mea. S_{22} denotes the measured reflection coefficient of slot 2. The simulated resonant frequency is 2.575 GHz, and the measured resonant frequencies of S_{11} and S_{22} are 2.49 GHz and 2.51 GHz, respectively. The difference between the simulated S_{11} and measured S_{11} is 3.07%. The difference between the simulated S_{22} and measured S_{22} is 2.43%. The difference between the measured S_{11} and S_{22} is 0.6%. There is acceptable agreement between the simulated and measured S-parameters.

Figure 15 shows the normalized radiation patterns in the E-plane and H-plane for the connection of MSs, when it operates in antenna mode. In this connection of MSs, slots 1 and 2 are fed by microstrip line 1 and microstrip line 2, respectively. Those slots radiate independently. Their radiation patterns were therefore measured independently. The measured E-plane radiation patterns are in good agreement with the simulated ones in the main beam direction. The main lobes of the H-plane radiation patterns, for slots 1 and 2, are tilted towards opposite directions, as expected. When slots 1 and 2 are excited, there will be an electric field distribution around slots 1 and 2. The mutual coupling between those two electric fields will cause the main beams from slots 1 and 2 to be tilted in the H-plane. There are many approaches for decoupling between resonators. One of those approaches could be used to decouple slot 1 from slot 2. For instance, one could increase the distance between slot 1 and slot 2; another approach is to employ additional transmission lines, which introduce out of phase coupling to cancel the mutual component of coupling [49]. However, adopting one of those approaches, in the proposed connection of MSs, would dramatically increase the complexity of the design process. It may also increase the insertion loss of this connection of MSs, when it is operating in filter mode. For these reasons, we decided not to employ a decoupling circuit. The simulated radiation efficiency for slots 1 and 2 is 84%. The simulated peak realized gain of slots 1 and 2 is 8.71 dBi. The measured peak realized gain is 7.19 dBi for slot 1 and 7.23 dBi for slot 2. Akin to the single MS, the discrepancy between the measured and simulated gains of the connection of MS is caused by assembly errors.

4.2. Resonator Mode MS and Filter Mode Connection of MSs

The proposed MS/connection of MSs can operate in resonator/filter mode when LM is injected into all of the fluidic channels and formed into 2D shapes. In order to realize 2D-shaped LM, we make use of Young-Laplace pressure to form LM. The Young-Laplace pressure can be expressed as

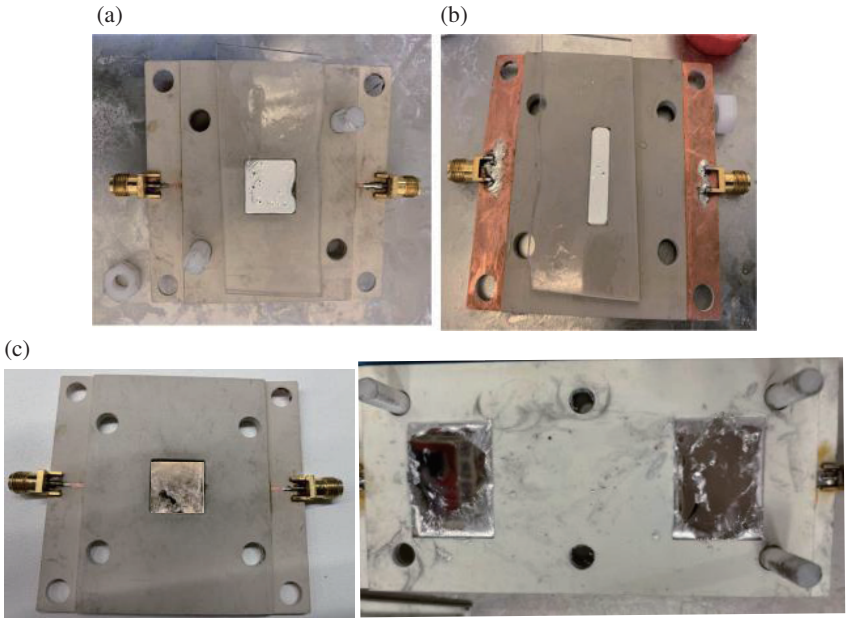

FIGURE 16. (a), (b) Filling fluidic channels with LM. (c) MS/connection of MSs in the resonator/filter mode.

follows:

$$P_{Laplace} = 2\sigma_l \cos\theta_l \left(\frac{1}{w_C} + \frac{1}{h_C}\right) \tag{2}$$

where σ_l is the surface tension of the liquid; θ_l is the contact angle between liquid metal and channel (which defaults as 90°); and w_C and h_C are LM curvature radiuses, which are equal to channel dimensions when channel is fully filled [46]. The method based on this equation is explained as follows:

LM is a non-Newtonian fluid. It means that the surface tension of LM is much higher than Newtonian fluid, e.g., water. From Equation (2) we understand that, when σ_l is high, the pressure difference between outside and inside of LM, namely $P_{Laplace}$, is high. A direct reflection of this feature is that when LM is dropped inside the channel, it will start shrinking towards the center of this channel. However, σ_l is gradually decreased during the surface oxidizing of LM [50, 51]. $P_{Laplace}$ is in turn gradually decreased. Consequently, shirking of the LM will be gradually slowing down until fixing to a certain volume. At this stage, $P_{Laplace}$ will equal the atmospheric pressure intensity.

In order to operate the MS/connection of MSs in resonator/filter mode, we need LM to be entirely filled into the fluidic channel for realizing 2D shapes. In other words, we want to prevent LM from shrinking. The most straightforward way to do this is to provide an external pressure to counteract $P_{Laplace}$. To this end, we simply use a small piece of Perspex to compress the LM (see Figs. 16(a) and (b)) after it is filled into fluidic channels. The Perspex does not insulate LM from air, which means that the surface oxidation of LM still happens. The $P_{Laplace}$ will eventually decrease to a value that akin to the atmospheric pressure intensity. When this is the case, LM will not shrink. Consequently, we can form LM into 2D geometrics, (see Fig. 16(c))). This 2D-shaped LM is mechanical stable, which is secured for vehicle-borne applications.

If we want to change the proposed MS/connection of MSs from resonator/filter mode back to antenna mode, we need to wash 2D-shaped LM out from fluidic channel. To do this, we use solutions such as sodium hydroxide (NaOH) or hydrochloride (HCL). Thanks to the open channels we propose that this cleaning process can be simply proceeded without leaving intuitional residues.

Figure 17 shows the simulated and measured S-parameters of the MS when it is operating in the resonator mode. The simulated resonant frequency is 2.52 GHz. The measured resonant frequency is 2.48 GHz. The difference between simulation and measurement is therefore 1.56%, which is acceptable. The simulated value of S_{11}, at the operating frequency of the MS when it functions in the resonator mode, is -18 dB. The measured value of S_{11}, at the operating frequency of the MS when it functions in the resonator mode, is -29 dB. The simulated insertion loss of the MS functioning in the resonator mode is 1.2 dB, whilst the measured insertion loss, for the same structure, is 1.8 dB. The simulation and measurement results agree well.

Figure 18 shows the simulated and measured S-parameters of the connection of MSs, when it is operating in the filter mode. The 10 dB return loss bandwidth of the simulated S_{11} extends from 2.1 GHz to 2.5 GHz. The 10 dB return loss bandwidth of the measured S_{11} extends from 2.28 GHz to 2.62 GHz, i.e., 13.8%. Within the passband of the filter the simulated S_{21} is seen to range from -2.8 dB to -1.2 dB. The measured S_{21} is seen to range from -3.4 dB to -1.9 dB. The out-of-band rejection of the filter has an average level of -20 dB. Recall that in the proposed connection of MSs, the coupling coefficient is determined by the distance between resonators, i.e., Dg. The coupling coefficient of this connection of MSs is thus not af-

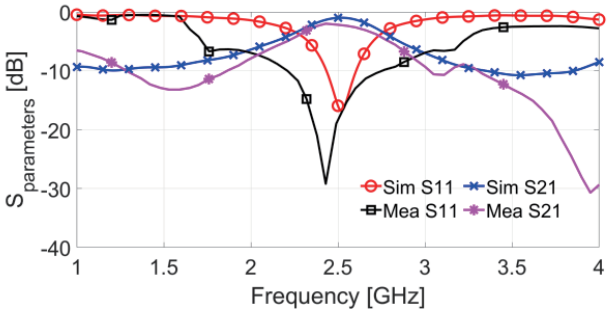

FIGURE 17. S-parameters for the MS operating in the resonator mode. Where: Sim. Means simulated and Meas. Means measured.

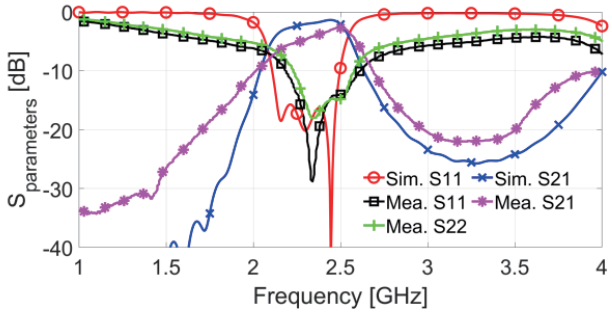

FIGURE 18. S-parameters for the connection of MSs operating in filter mode. Where: Sim. Means simulated and Meas. Means measured.

fected by LM. The quality factors of this connection of MSs, however, are mostly controlled by two LM bars, as discussed above. Those LM bars are formed by filling two very tiny fluidic channels with LM. The input/output quality factors of the connection of MSs is therefore affected by the exact amount of LM within the channels that form the bars. The consequence of this is that the lowermost and middle S_{11} zeros merge together. In turn, this reduces the passband bandwidth of the connection of MSs.

It should be noted that the proposed MS/connection of MSs do not consist of LM when they are operating in antenna mode. Therefore, the antenna mode performance of the proposed MS/connection of MSs is close to the performance of a typical slot antenna. On the other hand, Table 3 compares the performance of the proposed connection of MSs (filter mode) against the performance of some functional changeable subsystems that can be tuned to operate in filter mode. The minimum value of the insertion loss of the proposed subsystem is lower than that of all of the other competing function changeable subsystems, shown in Table 3. In addition, the instantaneous bandwidth of the proposed connection of MSs (filter mode) is wider than that of all of the function tunable subsystems listed in Table 3.

5. CONCLUSION

This paper presents the first microwave subsystem capable of changing its function, between resonator and antenna, using liquid metal (LM) [52]. Also, for the first time we use the oxide which forms on the surface of LM to stabilize it and assist in the creation of a patch resonator. Functional change is achieved by filling and emptying fluidic channels with LM. Specifically, the resonator mode of the proposed microwave subsystem (MS) is obtained when the fluidic channels are filled with LM. The antenna mode is obtained when all of the channels are emptied of LM. Two MSs and a microstrip patch resonator are then cascaded to form a connection of MSs that is capable of realizing more complex circuit and antenna functions. Specifically, filter mode is obtained when the fluidic channels, within the connection of MSs, are filled with LM. On the other hand, the antenna mode, for the connection of MSs, is obtained by emptying all of the channels. The proposed MS and connection of MSs yield good levels of performance. The proposed MS and connection of MSs is designed to be operated at 2.5 GHz. The MS has a peak realized gain of 7.81 dBi and a simulated total efficiency of 95%, when it is operating in the antenna mode. When the MS is operating in the resonator mode, it has a measured insertion loss of 1.8 dB. The proposed connection of MSs has a peak realized gain of 7.23 dBi and a total efficiency of 84% when it is operating in the antenna mode. The connection of MSs has a 10 dB return loss bandwidth of 340 MHz ranging from 2.28 GHz and 2.62 GHz when it is operating in filter mode.

ACKNOWLEDGEMENT

This work was supported by the U.K. Engineering and Physical Sciences Research Council [Grant number EP/V008420/1]. The author would like to thank to Max Munoz Torrico and Andre Saker Andy. Andy and Max are associated with the antenna lab of Queen Mary University of London and they kindly supported the experiment and measurement of the proposed hardware.

REFERENCES

[1] Chen, F.-C., H.-T. Hu, R.-S. Li, Q.-X. Chu, and M. J. Lancaster, "Design of filtering microstrip antenna array with reduced sidelobe level," *IEEE Transactions on Antennas and Propagation*, Vol. 65, No. 2, 903–908, 2016.

[2] Zheng, Z., X. Fang, W. Wang, G. Huang, H. Zhang, and X. Liang, "A compact waveguide slot filtering antenna based on mushroom-type surface," *IEEE Antennas and Wireless Propagation Letters*, Vol. 19, No. 10, 1823–1827, 2020.

[3] Wang, W., Z. Zheng, X. Fang, H. Zhang, M. Jin, J. Lu, Q. Luo, and S. Gao, "A waveguide slot filtering antenna with an embedded metamaterial structure," *IEEE Transactions on Antennas and Propagation*, Vol. 67, No. 5, 2953–2960, 2019.

[4] Mao, C.-X., S. Gao, Y. Wang, F. Qin, and Q.-X. Chu, "Multimode resonator-fed dual-polarized antenna array with enhanced bandwidth and selectivity," *IEEE Transactions on Antennas and Propagation*, Vol. 63, No. 12, 5492–5499, 2015.

[5] Lu, J., H. Zhang, W. Wang, X. Liang, J. Ge, M. Jin, and W. Wu, "Broadband dual-polarized waveguide slot filtenna array with

low cross polarization and high efficiency," *IEEE Transactions on Antennas and Propagation*, Vol. 67, No. 1, 151–159, 2018.

[6] Li, P. K., C. J. You, H. F. Yu, X. Li, Y. W. Yang, and J. H. Deng, "Codesigned high-efficiency single-layered substrate integrated waveguide filtering antenna with a controllable radiation null," *IEEE Antennas and Wireless Propagation Letters*, Vol. 17, No. 2, 295–298, 2017.

[7] Zhang, X. Y., W. Duan, and Y.-M. Pan, "High-gain filtering patch antenna without extra circuit," *IEEE Transactions on Antennas and Propagation*, Vol. 63, No. 12, 5883–5888, 2015.

[8] Chu, H., C. Jin, J.-X. Chen, and Y.-X. Guo, "A 3-D millimeter-wave filtering antenna with high selectivity and low cross-polarization," *IEEE Transactions on Antennas and Propagation*, Vol. 63, No. 5, 2375–2380, 2015.

[9] Duan, W., X. Y. Zhang, Y.-M. Pan, J.-X. Xu, and Q. Xue, "Dual-polarized filtering antenna with high selectivity and low cross polarization," *IEEE Transactions on Antennas and Propagation*, Vol. 64, No. 10, 4188–4196, 2016.

[10] Fang, X., W. Wang, G.-L. Huang, Q. Luo, and H. Zhang, "A wideband low-profile all-metal cavity slot antenna with filtering performance for space-borne SAR applications," *IEEE Antennas and Wireless Propagation Letters*, Vol. 18, No. 6, 1278–1282, 2019.

[11] Ahsan, N., A. Ouacha, C. Samuelsson, and T. Boman, "Applications of programmable microwave function array (PROMFA)," in *2007 18th European Conference on Circuit Theory and Design*, 164–167, 2007.

[12] Samuelsson, C., A. Ouacha, N. Ahsan, and T. Boman, "Programmable microwave function array, PROMFA," in *2006 Asia-pacific Microwave Conference*, 1787–1790, Yokohama, Japan, 2006.

[13] Kelly, J. R. and A. Borja, "Hardware block for use in programmable microwave function arrays," *Electronics Letters*, Vol. 50, No. 15, 1076–1077, 2014.

[14] Borja, A. L., Y. Kabiri, A. Belenguer, and J. R. Kelly, "Programmable multifunctional RF/microwave circuit for antenna and filter operation," *IEEE Transactions on Antennas and Propagation*, Vol. 66, No. 8, 3865–3876, 2018.

[15] Li, H.-Y., J.-X. Xu, Y. Yang, and X. Y. Zhang, "Novel switchable filtering circuit with function reconfigurability between SPQT filtering switch and four-way filtering power divider," *IEEE Transactions on Microwave Theory and Techniques*, Vol. 68, No. 3, 867–876, 2019.

[16] Lovato, R. and X. Gong, "A third-order SIW-integrated filter/antenna using two resonant cavities," *IEEE Antennas and Wireless Propagation Letters*, Vol. 17, No. 3, 505–508, 2018.

[17] Lai, J., T. Yang, P.-L. Chi, and R. Xu, "A novel 1.7-2.85-GHz filtering crossover with independently tuned channel passbands and reconfigurable filtering power-dividing function," *IEEE Transactions on Microwave Theory and Techniques*, Vol. 69, No. 5, 2458–2469, 2021.

[18] Zhu, X., T. Yang, P.-L. Chi, and R. Xu, "Novel tunable isolation network used in ring-type single-to-balanced, power-dividing, and single-ended filter with arbitrary power-division ratios," *IEEE Transactions on Microwave Theory and Techniques*, Vol. 68, No. 2, 666–680, 2019.

[19] Sang, L., X. Guo, J. Xu, X. Li, M. Kraman, Y. Mei, and W. Huang, "Antenna-filter-splitter function reconfigurable microwave passive device based on VO2," *IEEE Antennas and Wireless Propagation Letters*, Vol. 19, No. 10, 1654–1658, 2020.

[20] Lin, Y.-S., P.-S. Lu, and Y.-C. Wu, "A novel configurable microwave passive component based on programmable bridged-T coil array," *IEEE Transactions on Microwave Theory and Techniques*, Vol. 69, No. 6, 3001–3014, 2021.

[21] Yang, W. and C. Wang, "Graphene and the related conductive inks for flexible electronics," *Journal of Materials Chemistry C*, Vol. 4, 7193–7207, 2016.

[22] Sang, M., J. Shin, K. Kim, and K. J. Yu, "Electronic and thermal properties of graphene and recent advances in graphene based electronics applications," *Nanomaterials*, Vol. 9, No. 3, 374, 2019.

[23] Morishita, A. M., C. K. Y. Kitamura, A. T. Ohta, and W. A. Shiroma, "A liquid-metal monopole array with tunable frequency, gain, and beam steering," *IEEE Antennas and Wireless Propagation Letters*, Vol. 12, 1388–1391, 2013.

[24] Wang, M., I. M. Kilgore, M. B. Steer, and J. J. Adams, "Characterization of intermodulation distortion in reconfigurable liquid metal antennas," *IEEE Antennas and Wireless Propagation Letters*, Vol. 17, No. 2, 279–282, 2017.

[25] Alqurashi, K. Y., J. R. Kelly, Z. Wang, C. Crean, R. Mittra, M. Khalily, and Y. Gao, "Liquid metal bandwidth-reconfigurable antenna," *IEEE Antennas and Wireless Propagation Letters*, Vol. 19, No. 1, 218–222, 2019.

[26] Dey, A., R. Guldiken, and G. Mumcu, "Microfluidically reconfigured wideband frequency-tunable liquid-metal monopole antenna," *IEEE Transactions on Antennas and Propagation*, Vol. 64, No. 6, 2572–2576, 2016.

[27] Mazlouman, S. J., X. J. Jiang, A. N. Mahanfar, C. Menon, and R. G. Vaughan, "A reconfigurable patch antenna using liquid metal embedded in a silicone substrate," *IEEE Transactions on Antennas and Propagation*, Vol. 59, No. 12, 4406–4412, 2011.

[28] Chen, Z., H. Wong, and J. Kelly, "A polarization-reconfigurable glass dielectric resonator antenna using liquid metal," *IEEE Transactions on Antennas and Propagation*, Vol. 67, No. 5, 3427–3432, 2019.

[29] Rodrigo, D., L. Jofre, and B. A. Cetiner, "Circular beam-steering reconfigurable antenna with liquid metal parasitics," *IEEE Transactions on Antennas and Propagation*, Vol. 60, No. 4, 1796–1802, 2012.

[30] Alkaraki, S., J. Kelly, A. L. Borja, R. Mittra, and Y. Wang, "Gallium-based liquid metal substrate integrated waveguide switches," *IEEE Microwave and Wireless Components Letters*, Vol. 31, No. 3, 257–260, 2020.

[31] Alkaraki, S., A. L. Borja, J. R. Kelly, R. Mittra, and Y. Gao, "Reconfigurable liquid metal-based SIW phase shifter," *IEEE Transactions on Microwave Theory and Techniques*, Vol. 70, No. 1, 323–333, 2021.

[32] Zhu, X., F. Yang, S. Zhao, H. Wang, C. Niu, and M. Rong, "Liquid-metal capillary switch for electrical power application," *Applied Physics Letters*, Vol. 117, No. 26, 263701, 2020.

[33] Le Goff, D., Y. Quere, A. Maalouf, E. Rius, P. Coquet, and E. H. T. Teo, "Concept of vertical liquid metal actuated cyclo-olefin-polymer based embedded 360° steerable yagi-uda antenna," *Microwave and Optical Technology Letters*, Vol. 63, No. 5, 1514–1519, 2021.

[34] Abu Bakar, H., R. A. Rahim, P. J. Soh, and P. Akkaraekthalin, "Liquid-based reconfigurable antenna technology: Recent developments, challenges and future," *Sensors*, Vol. 21, No. 3, 827, 2021.

[35] Song, M., K. E. Daniels, A. Kiani, S. Rashid-Nadimi, and M. D. Dickey, "Interfacial tension modulation of liquid metal via electrochemical oxidation," *Advanced Intelligent Systems*, Vol. 3, No. 8, 2100024, 2021.

[36] Floc'h, J. M. and I. B. Trad, "Design of mechanically reconfigurable meander antenna using the Galinstan liquid metal," in *Loughborough Antennas & Propagation Conference (LAPC*

2017), Loughborough, UK, 2017.

[37] Song, L., W. Gao, C. O. Chui, and Y. Rahmat-Samii, "Wideband frequency reconfigurable patch antenna with switchable slots based on liquid metal and 3-D printed microfluidics," *IEEE Transactions on Antennas and Propagation*, Vol. 67, No. 5, 2886–2895, 2019.

[38] Song, L., W. Gao, and Y. Rahmat-Samii, "3D printing-based liquid metal patch antennas with wide-band frequency and multi-polarization reconfigurations," in *2019 URSI International Symposium on Electromagnetic Theory (EMTS)*, San Diego, CA, USA, 2019.

[39] Hayes, G. J., J.-H. So, A. Qusba, M. D. Dickey, and G. Lazzi, "Flexible liquid metal alloy (EGaIn) microstrip patch antenna," *IEEE Transactions on Antennas and Propagation*, Vol. 60, No. 5, 2151–2156, 2012.

[40] Alqurashi, K. and J. Kelly, "Continuously tunable frequency reconfigurable liquid metal patch antenna," in *IEEE International Symposium on Antennas and Propagation*, San Diego, CA, USA, 2017.

[41] Alqurashi, K. Y., C. Crean, J. R. Kelly, T. W. C. Brown, and M. Khalily, "Liquid metal application for continuously tunable frequency reconfigurable antenna," in *2019 13th European Conference on Antennas and Propagation (EUCAP)*, 1–3, Krakow, Poland, 2019.

[42] Zandvakili, M., M. M. Honari, P. Mousavi, and D. Sameoto, "Gecko-gaskets for multilayer, complex, and stretchable liquid metal microwave circuits and antennas," *Advanced Materials Technologies*, Vol. 2, No. 11, 1700144, 2017.

[43] Alqurashi, K. Y., "Liquid metal feasibility and characterisation in reconfigurable antenna applications," Ph.D. dissertation, Institu. Comm. Syst, Fac. Eng. Phy. Sci., Univ. Surrey, Surrey, England, 2019.

[44] Pozar, D. M., *Microwave Engineering*, 4th ed., John Wiley & Sons, Inc., 2005.

[45] Barbuto, M., A. Alu, F. Bilotti, A. Toscano, and L. Vegni, "Characteristic impedance of a microstrip line with a dielectric overlay," *Compel: The International Journal For Computation and Mathematics in Electrical and Electronic Engineering*, Vol. 32, No. 6, 1855–1867, 2013.

[46] Wang, C., J. C. Yeo, H. Chu, C. T. Lim, and Y.-X. Guo, "Design of a reconfigurable patch antenna using the movement of liquid metal," *IEEE Antennas and Wireless Propagation Letters*, Vol. 17, No. 6, 974–977, 2018.

[47] Hong, J.-S. G. and M. J. Lancaster, *Microstrip Filters For RF/Microwave Applications*, John Wiley & Sons, 2004.

[48] Balanis, C. A., *Antenna Theory: Analysis and Design*, John Wiley & Sons, 2016.

[49] Fang, X., G. Wen, D. Inserra, Y. Huang, and J. Li, "Compact wideband CPW-fed meandered-slot antenna with slotted Y-shaped central element for Wi-Fi, WiMAX, and 5G applications," *IEEE Transactions on Antennas and Propagation*, Vol. 66, No. 12, 7395–7399, 2018.

[50] Elton, E. S., T. C. Reeve, L. E. Thornley, I. D. Joshipura, P. H. Paul, A. J. Pascall, and J. R. Jeffries, "Dramatic effect of oxide on measured liquid metal rheology," *Journal of Rheology*, Vol. 64, No. 1, 119–128, 2020.

[51] Bark, H. and P. S. Lee, "Surface modification of liquid metal as an effective approach for deformable electronics and energy devices," *Chemical Science*, Vol. 12, No. 8, 2760–2777, 2021.

[52] Fang, X., "Programmable microwave devices (PMDs) based on liquid metal," Ph.D. dissertation, School of Electronic Engineering and Computer Science, Queen Mary University of London, London, England, 2023.